

UPDATES ON MODELING THE WATER CYCLE WITH THE NASA AMES MARS GLOBAL CLIMATE MODEL.

M. A. Kahre, NASA Ames Research Center, CA, USA (*melinda.a.kahre@nasa.gov*), **R. M. Haberle**, **J. L. Hollingsworth**, NASA Ames Research Center, CA, USA, **F. Montmessin**, Laboratoire Atmosphères, Milieux, Observations Spatiales, France, **A. S. Brecht**, **R. Urata**, BAER Institute / NASA Ames Research Center, CA, USA, **D. R. Klassen**, Rowan University, NJ, USA, **M. J. Wolff**, Space Science Institute, CO, USA.

Introduction:

Global Circulation Models (GCMs) have made steady progress in simulating the current Mars water cycle. It is now widely recognized that clouds are a critical component that can significantly affect the nature of the simulated water cycle. Two processes in particular are key to implementing clouds in a GCM: the microphysical processes of formation and dissipation, and their radiative effects on heating/cooling rates. Together, these processes alter the thermal structure, change the dynamics, and regulate inter-hemispheric transport. We have made considerable progress representing these processes in the NASA Ames GCM, particularly in the presence of radiatively active water ice clouds. We present the current state of our group's water cycle modeling efforts, show results from selected simulations, highlight some of the issues, and discuss avenues for further investigation.

Approach:

We use version 2.3 of the NASA Ames Mars Global Climate Model (GCM) to investigate the current Mars water cycle. The model uses an Arakawa-C horizontal grid with a nominal resolution of 5° in latitude and 6° in longitude. The vertical grid is a normalized sigma (terrain-following) coordinate with increasing layer thickness with altitude up to ~ 80 km. MOLA topography and thermal inertia and albedo maps derived from Viking and MGS/TES observations are used as surface boundary conditions. The model includes a Mellor and Yamada level-2 planetary boundary layer, a 2-stream radiation code that accounts for the radiative effects of CO_2 and H_2O gas and atmospheric aerosols, a sub-surface code that allows for heterogeneous soil properties, and a Van-Leer scheme for tracer transport.

Dust is required in the model for radiative forcing and to provide ice nuclei for water ice clouds. Column dust optical depths are defined by TES-observed MY 24 dust climatology maps of Montabone et al. (2015) binned to the model resolution. Dust is injected into the lowest atmospheric layer from the surface when the transported atmospheric dust optical depth drops below the TES-observed value for that location and season. These radiatively active dust particles are transported by model winds

and undergo gravitational sedimentation. Thus, we allow the model to self-consistently determine the dust particle vertical distribution.

We represent the Mars water cycle in the GCM by including water sublimation, water ice cloud nucleation, growth, transport, and sedimentation (Montmessin et al., 2002; 2004). The North Residual Cap (NRC) is assumed to be the only source of atmospheric water, and it is defined to be located where the observed surface thermal inertia exceeds 550 SI in the north polar region. We represent dust and cloud particle size distributions with the first two moments for computational efficiency. Simulated water ice clouds, particularly those that tend to form over the NRC during summer, can be quite sensitive to the time step used for the microphysical calculations. To mitigate this issue, we have implemented a time splitting scheme similar to the one described in Navarro et al. (2014). A key aspect of our implementation is that the water vapor and temperature changes that occur outside of the microphysics routine are fed incrementally into the microphysics time splitting loop. The time splitting scheme and incremental adjustments are the most important recent updates to the model.

Baseline Simulation:

We have found that careful tuning is required in addition to time-splitting in order to reasonably simulate the current Mars water cycle. As discussed in more detail below, the pattern and thickness of simulated clouds are extremely sensitive to tuning parameters (such as the contact parameter, m). Our baseline simulation has radiatively active clouds, a 30 second microphysical time step, and a contact parameter of 0.975. This simulation is initiated with a dry atmosphere and isothermal atmospheric temperatures. The surface and sub-surface temperatures are initiated with the zonal mean surface temperatures from a previous fully equilibrated simulation.

Results and Discussion:

Simulated Water Cycle Overview. Column water vapor and cloud fields from our baseline simulation are in generally good agreement with observations. Zonal mean water vapor column abundances maximize at high northern latitudes at ~ 55 μm during NH summer (Figure 1). The tropics and subtropics

are drier than the observations suggest; this result appears to be consistent with other GCM simulations that include radiatively active clouds and time splitting (Navarro et al., 2014).

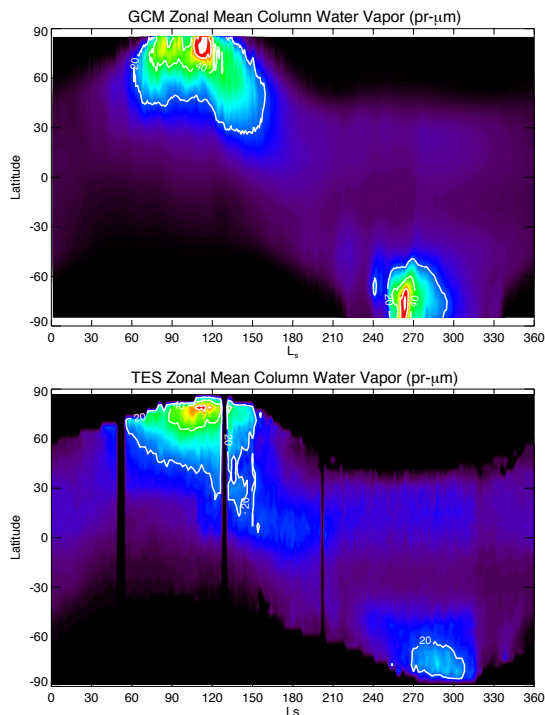


Figure 1: Zonal mean seasonally varying GCM-predicted (top) and TES-observed (bottom) water vapor column abundances.

Notably, there is a distinct gap in the clouds over the NRC from L_s 75° to 120° , but the clouds reappear in this simulation over the NRC earlier than the observations show (Figure 2). The predicted aphelion cloud belt (ACB) extends from L_s $\sim 60^\circ$ to $\sim 150^\circ$, is centered at $\sim 15^\circ$ N, and has peak zonally averaged IR (absorption-only) optical depths of ~ 0.12 . Peak predicted IR optical depths are $\sim 20\%$ lower than those observed by TES. We have found that it is difficult to predict clouds in the aphelion cloud belt that are thick enough in the IR compared to TES and at the same time prevent clouds from forming over the NRC throughout NH summer. Polar clouds are predicted in the vicinity of the seasonal CO_2 caps; the column thicknesses of these clouds are generally too thick compared to observations, which also appears to be a consistent feature of current water cycle GCMs.

Cloud Particle Sizes in the ACB. Utilizing observations in the IR from TES in combination with observations in the UV from MARCI allows us to put constraints on the cloud particles sizes in the aphelion cloud belt. As shown in the top panel of Figure 3, the predicted IR optical depths are lower than the IR-observed optical depths throughout the first half of the year, and the predicted UV optical depths are

consistently higher than the MARCI-observed UV optical depths. It is notable that the observed UV peak optical depth occurs slightly later in the season than the observed IR peak optical depth. The GCM does not capture this behavior.

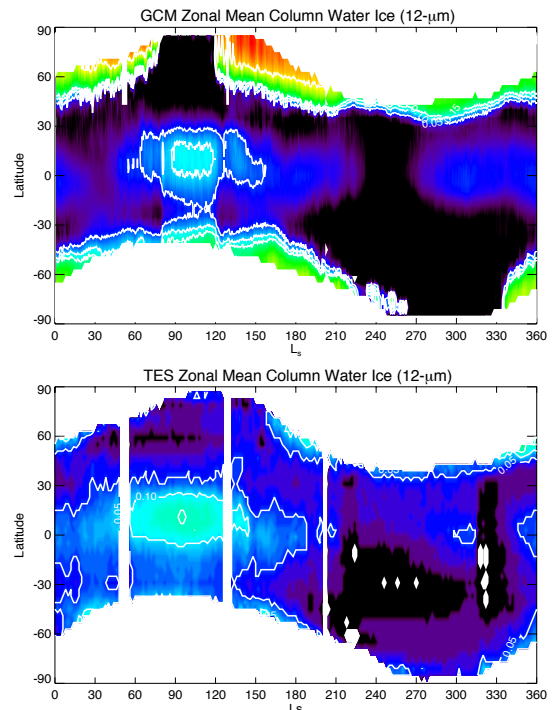


Figure 2: Zonal mean seasonally varying GCM-predicted (top) and TES-observed (bottom) water ice 12- μm absorption-only optical depths.

The bottom panel of Figure 3 shows the observed and GCM-predicted UV-to-IR (absorption only) ratios as a function of season. The observed UV-to-IR ratio is slightly less than one early in the year, and reaches ~ 1.5 during the peak thickness of the aphelion cloud belt (L_s 90° - 110°). The seasonal evolution in UV-to-IR ratio indicates that the cloud particle sizes change with season, with particles getting smaller as the cloud belt grows and then larger again as the cloud belt dissipates. The model-predicted UV-to-IR ratio at 10° N suggests that the model is not properly capturing realistic particle sizes. The high (compared to observations) predicted UV-to-IR ratio suggests that the model-predicted particle sizes are too small. Klassen et al. (this meeting) address this issue. This is an avenue we plan to focus on going forward in an effort to better understand the factors (number of cloud particles and water supply) that control the cloud particle sizes in the aphelion cloud belt.

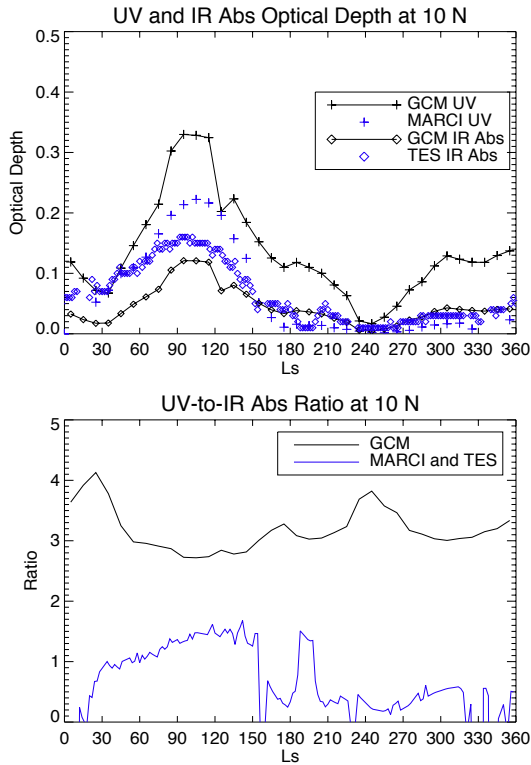


Figure 3: Observed and GCM-predicted UV and IR cloud optical depths (top) and UV-to-IR ratio (bottom) at 10 N as a function of season.

Vertical Extent of the ACB. MCS observations provide constraints on the vertical distribution of clouds in the aphelion cloud belt. Because MCS retrievals are not possible when the aerosol opacities are high, these observations are best used for constraining the altitude and structure of the top of the aphelion cloud belt.

As shown in Figure 4, MCS observations indicate that the top of the aphelion cloud belt resides at ~ 0.2 hPa (in the zonal mean), while the GCM predicts the top of the aphelion cloud belt to be much lower (~ 0.8 hPa). The GCM's inability to accurately predict the altitude of the top of the aphelion cloud belt is likely due to the relatively low horizontal resolution of the baseline simulation. As shown in Urata et al. (this meeting), even a modest increase in the spatial resolution allows for enhanced vertical transport of both water vapor and cloud that results in a more vertically extended cloud deck. Given the importance of clouds on net meridional transport (e.g., Clancy et al., 1995), this suggests that horizontal resolution may be more important than previously recognized.

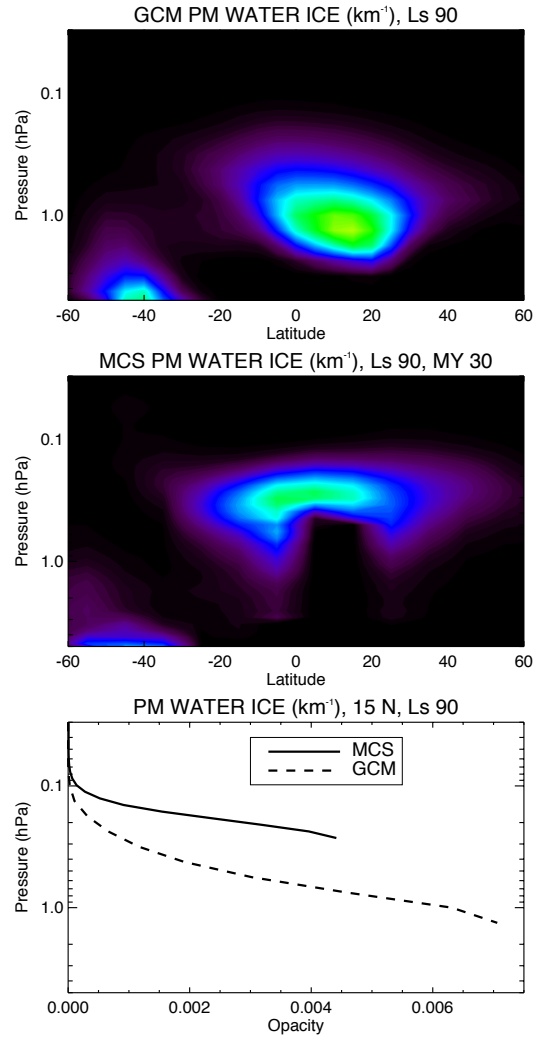


Figure 4: Zonal mean GCM-predicted (top) and MCS-observed (middle) water ice 12- μm opacities at L_s 90°. Profiles at 15 N (bottom).

Sensitivity of Clouds to the Contact Parameter. As stated earlier, a significant amount of tuning is required to produce a simulated water cycle that is in reasonably good agreement with the observations. We have found a large degree of sensitivity to one parameter in particular—the contact parameter (m), which effectively determines the critical supersaturation required for cloud nucleation. Laboratory studies suggest that the contact parameter is temperature-dependent for the temperatures present in the Martian atmosphere, although the relationship found differs amongst different studies (Trainer et al., 2009; Iraci et al., 2010). We have executed runs for a range of constant values (from 0.95 to 0.975) and for the temperature-dependent relationship found in the Trainer study. As shown in Figure 5, even this small range of constant contact parameter values produces significant differences in the thickness of the aphelion cloud belt. As the contact parameter decreases, the overall cloudiness of the atmosphere decreases significantly because higher saturations are

required for cloud nucleation so there is more growth on a fewer number of particles, which results in larger particles that fall quickly, either to the surface or to a sub-saturated region below. The $m=0.95$ case, for example, results in peak IR optical depths that are 50% less than those from our baseline case ($m=0.975$). The temperature-dependent contact parameter case results in very few clouds anywhere. Because the predicted cloud behavior is so sensitive to this parameter, continued laboratory work designed to put more definitive constraints on its value and temperature-dependence will be of vital importance.

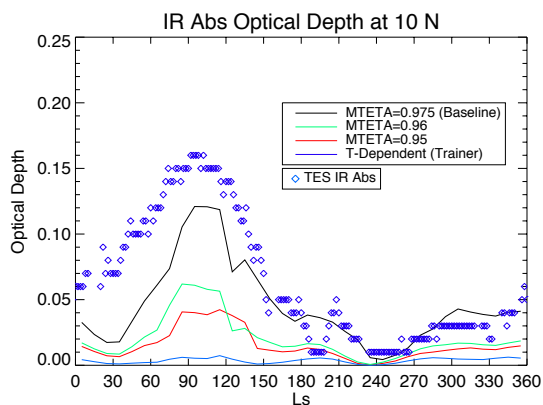


Figure 5: GCM-predicted IR cloud optical depths at 10 N as a function of season for different contact parameter sensitivity simulations.

Conclusions:

Although it is now possible to reasonably simulate many general aspects of the current Mars water cycle with the inclusion of water ice cloud radiative effects, it is clear that there are many details of the water cycle that are not yet well-reproduced. Cloud particle sizes and the vertical extent of the aphelion cloud deck are two areas that require further work. Consistent with other contemporary models, our model predicts dry tropics throughout much of the year. This is also an area that needs to be understood.

Finally, we note that the high degree of tuning that is required for even decent (not perfect) agreement with the observations is disconcerting. While our approach to modeling the water cycle is very similar to all other modeling groups that we are aware of, we are concerned about its robustness going forward.

References:

- Clancy et al. (1995), *JGR*, 101.
- Iraci et al. (2010), *Icarus*, 210.
- Klassen et al. (2016), this meeting.
- Montabone et al. (2015), *Icarus*, 251.
- Montmessin et al. (2002), *JGR*, 107.
- Montmessin et al. (2004), *JGR*, 109.
- Navarro et al. (2015), *JGR*, 119.
- Trainer et al. (2009), *J. Phys. Chem.* 113
- Urata et al. (2016), this meeting.